Journal of Photochemistry and Photobiology A: Chemistry 219 (2011) 90–100

Contents lists available at ScienceDirect

Journal of Photochemistry and Photobiology A: Chemistry

journal homepage: www.elsevier.com/locate/jphotochem

Fluorescence and conformation in water-soluble bis(pyrenyl amide) receptors derived from polyaminopolycarboxylic acids

Refugio Pérez-González [a], Lorena Machi [a,*], Motomichi Inoue [a], Mario Sánchez [b], Felipe Medrano [c]

[a] Departamento de Investigación en Polímeros y Materiales, Universidad de Sonora, Hermosillo, Sonora 83000, Mexico
[b] Centro de Investigación en Materiales Avanzados, S.C., Alianza Norte # 202, Autopista Nueva al Aeropuerto Km. 9.5, Apodaca, Nuevo León 66600, Mexico
[c] Centro de Investigaciones Químicas, Universidad Autónoma del Estado de Morelos, Av. Universidad 1001, Col. Chamilpa, Cuernavaca, Morelos 62209, Mexico

ARTICLE INFO

Article history:
Received 28 October 2010
Received in revised form 7 January 2011
Accepted 27 January 2011
Available online 2 February 2011

Keywords:
Bichromophores
Fluorescence
pH sensors
Pyrene derivatives
EDTA
Polyaminopolycarboxylic acids

ABSTRACT

Fluorescent responses and conformational changes against pH were studied on four new water-soluble 1-pyrene and 1-methylpyrene bichromophores, (ttha1py)H_4, (edta1mpy)H_2, (dtpa1mpy)H_3 and (ttha1mpy)H_4, with the objective of modifying pH–fluorescence profiles and other solution properties of 1-pyrene bichromophores, (edta1py)H_2 and (dtpa1py)H_3, developed previously by our group; the abbreviations with acidic protons stand for pyrenyl moieties interlinked by an EDTA, DTPA (diethylenetriaminepentacetic acid) or TTHA (triethylenetetraminehexaacetic acid) chain through amide linkages. The new derivatives exhibit emission bands of monomeric pyrene and an intense structureless excimer band; the latter responds to pH sensitively. The pH dependence of the emission intensity of the DTPA and TTHA derivatives is well correlated with species distribution determined by potentiometry. In every derivative, the completely deprotonated species L^{n-} is the most efficient for excimer emission, followed by the corresponding monoprotonated species $LH^{(n-1)-}$. In the latter, the acidic hydrogen is located on the central amine, as confirmed by ^{1}H NMR. The resulting hydrogen bond between amino nitrogen atoms makes the aliphatic chain rigid. Further protonation stretches the interlinking chain due to electrostatic repulsion. These conformational changes with protonation result in fluorescent on–off cycles against pH window. The switching cycles of the methylpyrene derivatives are reverse to those of the corresponding pyrene derivatives, as the CH_2 spacer between the amide and aromatic groups defines the orientation of pyrene rings. The sensitiveness of amide group to environment leads to a sharp change in excimer emission above pH ~11. The combined functions of amide and amino groups lead to the novel pH-responses.

1. Introduction

The design and syntheses of fluorescence probes based on pyrene have attracted considerable attention over the past 20 years [1–10]. A high quantum yield of fluorescence emission (Φ_{EtOH} = 0.65), a long lifetime of the singlet excited state (τ_s = 410 ns) and the ability to form excimers are some of the features that make pyrene one of the most useful chromophores for the construction of fluorogenic chemosensors for a variety of important chemical species. Particularly, the introduction of two pyrene moieties at the ends of interlinking chains containing electron-donating atoms has given a number of sensing systems capable of switching the monomer/excimer emission upon coordination with specific guest ions (M^{n+}, A^-, etc.). However, most of these systems act only in organic [11–22] or organic/aqueous-mixed media [23,24]. This characteristic limits their applications in biological, medical and environmental fields. To the best of our knowledge, to date there are only two reports of pyrene bichromophores acting in pure aqueous media in which excimer-to-monomer interconvertion is permitted by effect of pH or metal cations: a diethylenetriamine bearing two pyrene fragments at the respective ends, reported by Shiraishi et al. [25,26], and pyrene-based bichromophores **1** and **2** in Scheme 1, abbreviated as (edta1py)H_2 and (dtpa1py)H_3, respectively, reported recently by our group [27]. In compounds **1** and **2**, the anionic carboxylate arms in the EDTA (ethylenediaminetetraacetic acid) and DTPA (diethylenetriaminepentaacetic acid) interlinking chains endow the compounds with high water solubility in a wide pH range, and the multiple functional sites, including amino and amide nitrogen atoms, provide them with highly pH-sensitive fluorescent properties. The intense excimer emission of the EDTA derivative **1** observed in a basic medium (pH ≥ 9) is weakened sharply with decreasing pH in a narrow pH range, giving an striking "off–on" fluorescent profile associated with protonation of amino nitrogen in the

* Corresponding author. Tel.: +52 662 2592161.
E-mail address: lmachi@polimeros.uson.mx (L. Machi).

1010-6030/$ – see front matter © 2011 Elsevier B.V. All rights reserved.
doi:10.1016/j.jphotochem.2011.01.022

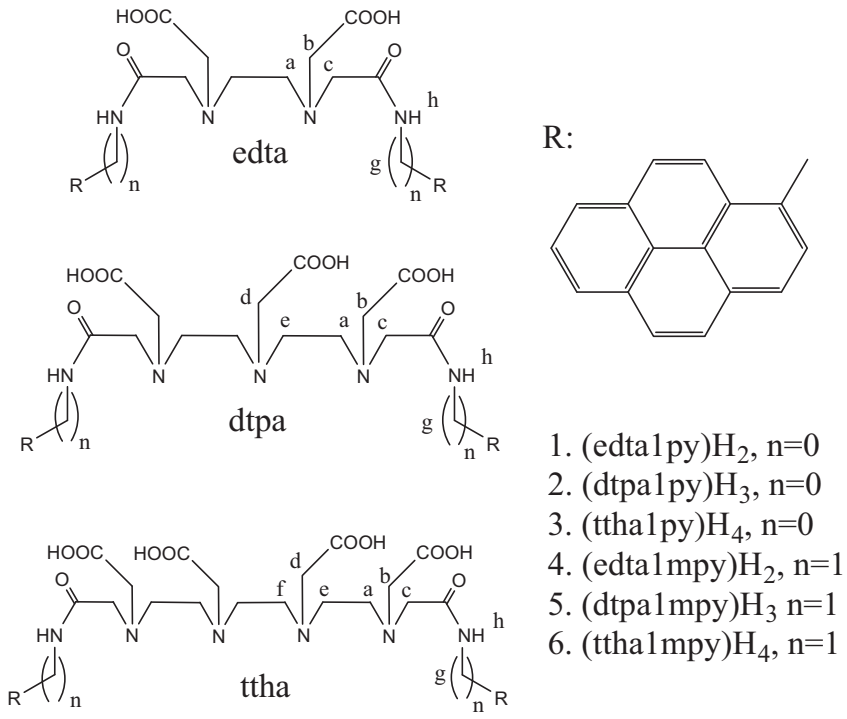

Scheme 1.

totally deprotonated species $(edta1py)^{2-}$. The DTPA derivative **2** also exhibits a strong excimer emission with an intensity–pH profile of an "off–on–off–on" type. This pH response is due to conformational changes induced by protonation–deprotonation processes in the DTPA interlinking chain, as has been confirmed by ^{1}H NMR [27]. The novel pH-sensing capabilities found for derivatives **1** and **2**, together with the increasing demand of molecular systems that behave as fluorescent indicators of the pH window, have prompted us to design bichromophores that have more intense emission, better pH specificity and higher water solubility. The present paper reports four new pyrene- and methylpyrene-based bichromophores (**3**–**6** in Scheme 1) composed of polyaminopolycarboxylate interlinks, EDTA, DTPA and TTHA (triethylenetetraminehexaacetic acid); the point of the molecular design includes (1) the introduction of a methylene spacer between amide and pyrenyl groups to enhance the emission and control the geometry, and (2) the employment of TTHA involving a larger number of donor atoms and hydrophilic groups to improve pH-response and water solubility. Compounds **3**–**6** abbreviated as $(ttha1py)H_4$, $(edta1mpy)H_2$, $(dtpa1mpy)H_3$ and $(ttha1mpy)H_4$, respectively, with acidic hydrogen exhibit an intense excimer emission which sensitively responds to pH with distinct intensity–pH profiles. The novel pH responses have been consistently interpreted by potentiometry, ^{1}H NMR, excitation spectra and density functional theory (DFT) calculations.

2. Experimental

2.1. Materials

EDTA dianhydride, 1-aminopyrene and 1-pyrenylmethylammonium hydrochloride were supplied from Aldrich. DTPA dianhydride and triethylenetetramine-N,N,N′,N″,N‴,N‴-hexaacetic acid (TTHA) were supplied from Sigma. These chemicals were used as received. Dimethylformamide (DMF) and pyridine were reagent grade and dried with molecular sieve 0.4 nm before use.

2.2. Synthesis of compounds

2.2.1. Synthesis of $(edta1mpy)H_2$: 1,4-bis(methylenecarboxy)-1,4-bis(N-1-pyrenylmethylacetamide)-1,4-diazabutane

$(Edta1mpy)H_2$ was synthesized by adding solid EDTA dianhydride (0.25 g, 0.97 mmol) little by little through a powder-dispensing funnel to a dimethylformamide (DMF, 25 mL) solution containing 1-pyrenylmethylammonium hydrochloride (0.64 g, 2.4 mmol) and triethylamine (350 μL, 2.5 mmol) with stirring under a nitrogen atmosphere. The resulting reaction mixture was left to stand overnight at room temperature. A light yellow solid formed was collected by filtration, washed thoroughly with ethanol in a Soxhlet extractor until decoloration, and dried in vacuum (0.31 g, 45%). M.p. 253–255 °C (dec). ^{1}H NMR (400 MHz, DMSO-d_6, TMS): δ = 2.774 (s, 4H, H_a), 4.965 (br, 4H, H_g), 8.721 (br, 2H, H_h), 7.962–8.280 (m, 18H, ArH), other proton signals were masked by HDO signal; MS (ESI) m/z (%): 719.3 (100) $[(M+H)^+]$; elemental analysis calcd (%) for $C_{44}H_{38}N_4O_6{\cdot}0.5H_2O$: C, 72.61; H, 5.40; N, 7.70; found: C, 72.73; H, 5.47; N, 7.74.

2.2.2. Synthesis of $(dtpa1mpy)H_3$: 1,4,7-tris(methylenecarboxy)-1,7-bis(N-1-pyrenylmethylacetamide)-1,4,7-triazaheptane

$(Dtpa1mpy)H_3$ was synthesized by essentially the same method as for $(edta1mpy)H_2$ from DTPA dianhydride (0.20 g, 0.56 mmol) and 1-pyrenylmethylammonium hydrochloride (0.37 g, 1.4 mmol) in the presence of triethylamine (195 μL, 1.5 mmol) in DMF (25 mL). After the resulting reaction mixture was left to stand overnight at room temperature, a small amount of solid formed was removed by filtration. The filtrate was concentrated to a viscous liquid. Addition of acetone (50 mL) to the concentrate yielded a green solid, which was separated by filtration, washed thoroughly with acetone in a Soxhlet extractor until decoloration, and dried in vacuum (0.30 g, 60%). M.p. 185–187 °C (dec). ^{1}H NMR (400 MHz, D_2O, DSS, pD = 10.5): δ = 2.083 (br, 8H, $H_{a,e}$), 2.756 (br, 4H, H_b), 2.899 (br, 6H, $H_{c,d}$), 4.248 (br, 4H, H_g), 7.001–7.311 (br m, 18H, ArH); MS (ESI) m/z (%): 820.3 (100) $[(M+H)^+]$; elemental analysis calcd (%) for $C_{48}H_{45}N_5O_8{\cdot}H_2O$:

C, 68.80; H, 5.65; N, 8.36; found: C, 68.72; H, 5.45; N, 8.45.

2.2.3. Synthesis of triethylenetetraminetetraacetic dianhydride, TTHA dianhydride

TTHA dianhydride was prepared according to the method reported by Achour et al. [28]. To TTHA (0.67 g, 1.35 mmol) were added acetic anhydride (1.00 mL, 10.6 mmol) and pyridine (0.67 mL, 8.20 mmol). The mixture was stirred at 40 °C for 48 h and filtered. The creamy precipitate was washed with acetic anhydride (100 mL) and then diethyl ether (100 mL), and dried under vacuum at 40 °C (0.58 g, 95%). The formation of the dianhydride was confirmed by the IR spectrum. The product was used without purification for the syntheses of the bis(pyrenyl amide) derivatives. IR (ν/cm^{-1}): 2698, 2922 (CH alkyl), 1780, 1920 (CO anhydride).

2.2.4. Synthesis of (ttha1py)H_4: 1,4,7,10-tetra(methylenecarboxy)-1,10-bis(N-1-pyrenylacetamide)-1,4,7,10-tetraazadecane

(Ttha1py)H_4 was synthesized by a method similar to that for (dtpa1py)H_3 [27]. TTHA dianhydride (0.65 g, 1.42 mmol) was added little by little through a powder-dispensing funnel to 1-aminopyrene (0.77 g, 3.5 mmol) in DMF (15 mL) at room temperature with stirring under a nitrogen atmosphere. The resulting reaction mixture was left to stand overnight at room temperature. Any solid present was removed by filtration, and the solution was concentrated to a viscous liquid. Addition of acetone (25 mL) to the concentrate yielded a green solid, which was separated by filtration, washed thoroughly with acetone in a Soxhlet extractor until decoloration, and dried in vacuum (0.44 g, 45.3%). M.p. 220–222 °C. ^{1}H NMR (400 MHz, D_2O, DSS, pD = 10.2): δ = 3.066 (br, 6H, $H_{a,e,f}$), 3.384 (s, 4H, H_d), 3.537 (s, 4H, H_b), 3.592 (s, 4H, H_c), 7.340–7.803 (m, 18H, ArH); MS (ESI) m/z (%): 893.3 (100) [(M+H)$^+$]; elemental analysis calcd (%) for $C_{50}H_{48}N_6O_{10}\cdot 1.5H_2O$: C, 65.27; H, 5.58; N, 9.13; found: C, 65.31; H, 5.42; N, 9.19.

2.2.5. Synthesis of (ttha1mpy)H_4: 1,4,7,10-tetra(methylenecarboxy)-1,10-bis(N-1-pyrenylmethylacetamide)-1,4,7,10-tetraazadecane

(Ttha1mpy)H_4 was synthesized by essentially the same method as for (dtpa1mpy)H_2 from TTHA dianhydride (0.50 g, 1.09 mmol) and 1-pyrenylmethylammonium hydrochloride (0.73 g, 2.72 mmol) in the presence of triethylamine (400 μL, 2.87 mmol) in DMF (25 mL). A small amount of solid formed at the end of the reaction was removed by filtration, and the solution was concentrated to a viscous liquid. Addition of acetone (50 mL) to the concentrate yielded a green solid, which was separated by filtration, washed thoroughly with acetone in a Soxhlet extractor until decoloration, and dried in vacuum. The resulting solid was suspended in 60 mL of water and dissolved by adding a minimum amount of solid Na_2CO_3. When the solution, after being filtered, was acidified to pH 4 with diluted HCl, a pale brown solid was formed, which was collected by centrifugation, washed with copious amounts of water and dried in vacuum. The solid was dissolved again in water with Na_2CO_3, and any insoluble substance was removed by filtration. Acidification of the resulting clear solution to pH 2 gave (ttha1mpy)H_4 in the acid form as a pale brown solid, which was separated by centrifugation, washed thoroughly with water and dried in vaccum (0.128 g, 13%). M.p. 145–147 °C. ^{1}H NMR (400 MHz, D_2O, DSS, pD = 10.1): δ = 0.379 (s, 4H, H_f), δ = 1.588 (br, 4H, H_a), 1.828 (br, 4H, H_e), 2.096 (s, 4H, H_d), 2.938 (s, 4H, H_b), 2.996 (s, 4H, H_c), 4.556 (s, 4H, H_g), 7.075-7.401 (m, 18H, ArH); MS (ESI) m/z (%): 921.2 (100) [(M+H)$^+$]; elemental analysis calcd (%) for $C_{52}H_{52}N_6O_{10}\cdot 2.5H_2O$: C, 64.65; H, 5.95; N, 8.70; found: C, 64.59; H; 5.93; N, 8.53.

2.3. Spectroscopic measurements

Luminescence spectra were recorded on a Perkin-Elmer LS-50B luminescence spectrometer. For experiments of pH dependence, sample compounds were dissolved in 0.01 M NaCl solution by adding an equimolar amount of solid Na_2CO_3, and the pH values of the sample solutions were adjusted with 0.01 M HCl and 0.01 M NaOH in such a way that the sample concentration as well as the ionic strength was identical for all solutions. Absorption spectra were obtained with a Perkin-Elmer Lambda 20 UV–Vis spectrometer. Sample solutions were prepared by the same procedure as for the fluorescence measurements. The ^{1}H NMR spectra were obtained with a Brucker AVANCE 400 spectrometer at a probe temperature of approximately 23 °C. In the studies of pD dependence, the pD range was limited because the water solubility of the compounds decrease sharply with decreasing pD: (dtpa1mpy)H_3 and (ttha1py)H_4 were studied at a concentration of 0.25 mmol kg^{-1} in the pD ranges of 8.0–13.0 and of 9.5–13.0, respectively; for (ttha1mpy)H_4 the concentration was 0.5 mmol kg^{-1} and the pD range was 8.0–13.0. Sample solutions were prepared as follows. Two stock solutions were prepared by adding a minimal amount of solid Na_2CO_3 into suspension of a sample compound in D_2O containing 0.01% DSS (sodium 2,2-dimethyl-2-silapentane-5-sulfonate) as the internal reference, followed by adjusting the pD to the lowest and the highest values with dilute solutions of HCl-*d* and KOH-*d* in D_2O, respectively. Sample solutions were prepared by weighing out the stock solutions directly into NMR sample tubes in different ratios in such a way that the total weight of every sample solution was 0.5 g. The pD value of each sample solution was determined by inserting an Aldrich ultra-thin long-stem combination electrode into the sample tube after NMR measurements. The electrode was calibrated with standard aqueous buffers in advance, and a pH value measured with a Corning 440 pH meter was converted to the pD value on the basis of the relation pD = pH_{meas} + 0.45 [29]. The EDTA derivative has too low a water solubility (<0.1 mmol kg^{-1} even at high pD) for reliable NMR experiments in D_2O. The mass spectra were obtained for methanol solutions at the University of Arizona Mass Spectroscopy Facility (Tucson, AZ, USA). The elemental analyses were performed by Columbia Analytical Service (Tucson, AZ, USA).

2.4. Potentiometric measurements

The determination of protonation constants was performed by potentiometry with a SCHOTT TITRONIC BASIC semiautomatic titrator consisting of a 20 mL-capacity Metrohm piston burette and a water-jacketed titration cell, and pH was measured with a Thermo Orion model 920A-plus pH meter equipped with an Orion 8102U combination electrode. The glass electrode was calibrated as a hydrogen-ion concentration probe by titrating 0.1 M HCl with CO_2-free 0.1 M NaOH. The equivalent point was determined by Gran's method, which gave pK_w 14.00. A sample solution (0.5 mM) was prepared by dissolving an appropriate sample compound with the calculated equivalent amount of 0.1 M NaOH, and titrated with ca. 0.1 M HCl. All calibrations and titrations were carried out under a CO_2-free nitrogen atmosphere at 25.0 ± 0.1 °C at an ionic strength of 0.10 M (NaCl). The NaOH and HCl solutions were standardized against potassium hydrogen phthalate and TRIS, respectively. Analysis of the data was performed by using the HYPERQUAD2006 v3.1.48 computer program. Species distribution diagrams were calculated with HYSS 2000 software. For each compound, logarithmic protonation constants (log K_p) were determined from three independent titrations. Since the pH titration range of each titration was limited because of the low solubility at low pH values, the number of protonation equilibria detected in the titration was varied; two to four protonation constants were determined for each com-

Table 1
Logarithms of the stepwise protonation constants of compounds **2**, **3**, **5** and **6** determined in aqueous NaCl (0.1 M) solution at 298 K.

L	Reaction[a]			
	H + L = HL	H + HL = H_2L	H + H_2L = H_3L	H + H_3L = H_4L
(dtpa1py)H_3	9.21 ± 0.01	5.35 ± 0.04	4.62 ± 0.03	–
(dtpa1mpy)H_3	9.95 ± 0.02	6.04 ± 0.08	nd[b]	–
(ttha1py)H_4	9.75 ± 0.02	6.75 ± 0.02	5.29 ± 0.02	4.68 ± 0.02
(ttha1mpy)H_4	10.24 ± 0.03	6.82 ± 0.05	4.99 ± 0.07	4.12 ± 0.1

[a] Charges are omitted for clarity.
[b] Undeterminable because of the low solubility in the corresponding pH range.

pound even when its molecular formula involves the larger number of acidic protons.

3. Results and discussion

3.1. Luminescence of (dtpa1mpy)H_3

A reaction between DTPA dianhydride and 1-aminomethylpyrene yields a 1:2 addition product abbreviated as (dtpa1mpy)H_3 (**5** in Scheme 1), whose solubility is about 0.5 mM (mM = 10^{-3} mol dm^{-3}) in strongly basic solution and it decreases sharply with decreasing pH. Common pyrene derivates have low water-solubility, which causes difficulty in characterization. The relatively high solubility of (dtpa1mpy)H_3 makes possible the studies of potentiometry and NMR, facilitating interpretation of the emission properties, although the pH range is limited. Potentiometric titration was able to be performed down to pH ~5, and the first and the second logarithmic protonation constants were determined as $\log K_{p1}$ = 9.95 and $\log K_{p2}$ = 6.04 (Table 1).

The fluorescence emission is so strong as to be observable at a concentration of 10^{-6} M down to pH 2. A broad band characteristic of pyrene excimer is observed at 484 nm, in addition to a set of sharp bands attributed to monomeric pyrene at 379 and 395 nm, as shown in Fig. 1. The excimer emission is strengthened sharply with increasing pH, while the monomer emission is less sensitive to pH. As shown in Fig. 2, the intensity of the excimer emission I_E is correlated to the species distribution, which is calculated from the protonation constants determined by potentiometry. The emission intensity I is given by an average over protonated species $LH_n^{(3-n)-}$ as a function of pH:

$$I = \frac{I_0 + \sum I_n \beta_n 10^{-n\,\mathrm{pH}}}{1 + \sum \beta_n 10^{-n\,\mathrm{pH}}} \quad (1)$$

Here, I_n is the intensity inherent in $LH_n^{(3-n)-}$, and β_n is the overall protonation constant, $\log \beta_n = \Sigma \log K_{pn}$. Curve fitting based on Eq. (1) was performed by a non-linear least-squares method [30]. The observed I_E vs. pH curve is reproduced well over the entire pH range with the logarithmic protonation constants, $\log K_{p1}$ = 10.17, $\log K_{p2}$ = 5.85, $\log K_{p3}$ = 5.09 and $\log K_{p4}$ = 2.91 (Fig. 2 and Table 2). The third and fourth protonations were detected by fluorometry thanks to the lower sample concentration necessary for the technique. The mol fractions based on the fluorometric data are presented by dashed lines in Fig. 2; the species distribution agrees well with that obtained from the potentiometric data. The relative intensity I_E inherent in each species is presented in Table 2; the species of the most efficient emission is the totally deprotonated species L^{3-}, and the second is LH_2^-.

The intensity–pH profile of (dtpa1mpy)H_3 is significantly different from that reported for (dtpa1py)H_3 (**2** in Scheme 1) [27]. The protonation constants of the latter have been determined by potentiometry in the present work as $\log K_{p1}$ = 9.21, $\log K_{p2}$ = 5.35 and $\log K_{p3}$ = 4.62 (Table 1). The species distribution presented in Fig. 3 shows that the LH^{2-} species is responsible for the most intense emission at pH ~8. Above this pH the emission is weakened as the L^{3-} species is formed, and then strengthened again with increas-

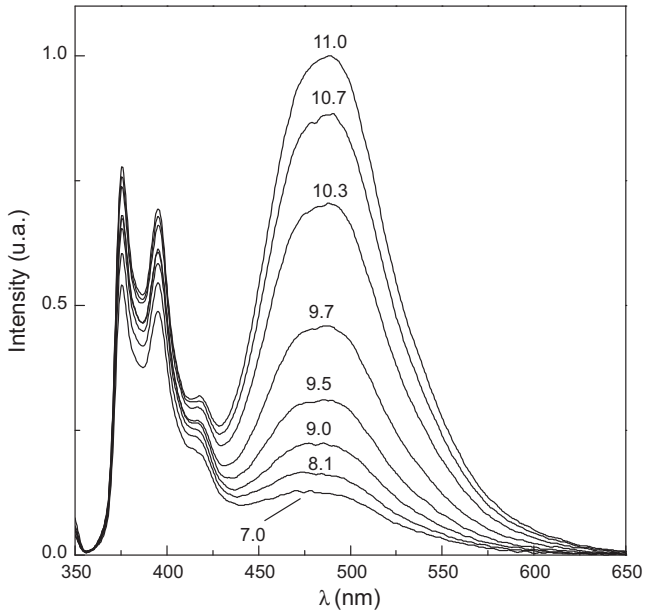

Fig. 1. Emission spectra of (dtpa1mpy)H_3 in aqueous solution at selected pH values. The spectral intensities are normalized to the peak maximum of the most intense spectrum. The excitation wavelength, λ_{exc} is 342 nm, and the concentration 1×10^{-6} M.

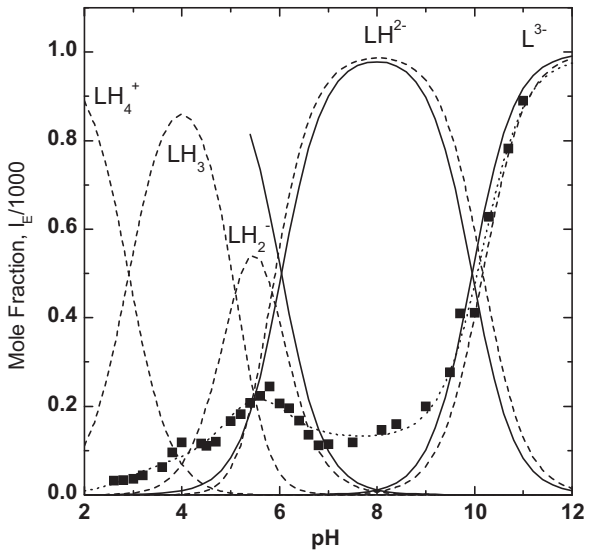

Fig. 2. Excimer emission intensity I_E (squares) of (dtpa1mpy)H_3 as a function of pH; the dotted line is the best fit based on Eq. (1) with $\log K_p$ values shown in Table 2. The mole fractions of the different species are determined by potentiometry (solid lines) and fluorometry (dashed lines).

Table 2
Logarithms of the protonation constants determined by fluorescence (in parenthesis) for compounds **1**–**6**, and relative fluorescence intensity inherent in each species with reference to the intensity of LH species.[a]

L	L_b	L_a (log K_{ab})	LH (log Kp_1)	LH_2 (log Kp_2)	LH_3 (log Kp_3)	LH_4 (log Kp_4)	LH_5 (log Kp_5)
(edta1py)H_2	590	244	1	–	–	–	–
		(−12.3)	(8.19)	nd[b]	–	–	–
(edta1mpy)H_2	~14000	2.05	1	–	~120	–	–
		(−14.6)	(7.43)	nd[b]	(~0.1)	–	–
(dtpa1py)H_3	3	0.4	1	0.1	–	–	–
		(−12.5)	(9.28)	(6.32)	nd[b]	nd[b]	–
(dtpa1mpy)H_3	nd[c]	8	1	2	1	0.01	–
	–	–	(10.17)	(5.85)	(5.09)	(2.91)	–
(ttha1py)H_4	4	0.02	1	0.6	0.2	0.4	<0.001
	–	(−11.0)	(10.29)	(6.86)	(5.38)	(5.06)	(1.8)
(ttha1mpy)H_4	30	3	1	0.6	–	–	0.2
	–	(−12.5)	(10.02)	(6.66)	nd[b]	nd[b]	(2.7)

[a] Charges are omitted for clarity.
[b] Not determinable due to small changes in fluorescence in the corresponding pH range.
[c] Conversion between L_a and L_b is not detected.

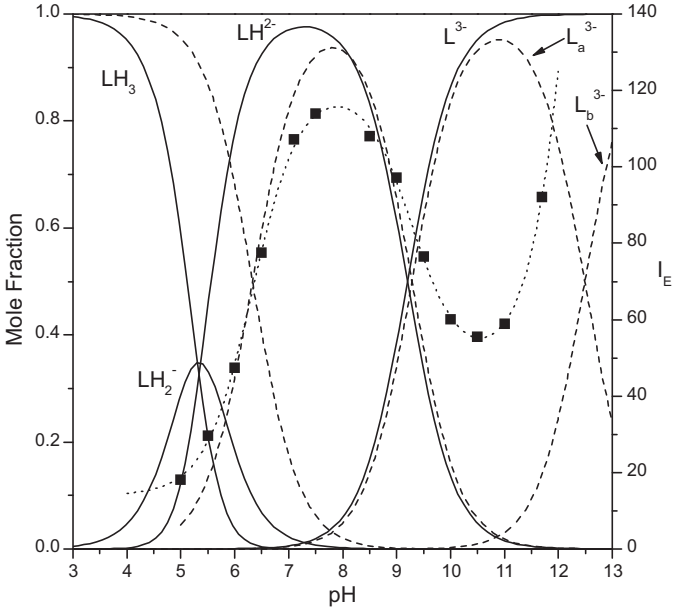

Fig. 3. Excimer emission intensity I_E (squares) of (dtpa1py)H_3 as a function of pH, and the species distributions determined by potentiometry (solid lines) and fluorometry (dashed lines). The dotted line is the best fit obtained by Eq. (3); the log K_p values are shown in Tables 1 and 2.

ing pH above pH 10.5. This increase of I_E in the high pH region is interpreted by the sensitiveness of the amide group to environmental changes because ^{1}H NMR does not show any shift in the corresponding pD range [27]; the completely deprotonated species $(dtpa1py)^{3-}$ takes two states, L_a^{3-} and L_b^{3-}, whose emission intensities are different from each other due to the amide effect. The conversion from L_a^{3-} to L_b^{3-} with pH is supposed to be formulated by the logistic (or the so-called dose–response) equation against pH. The mol fraction of L_b^{3-} is given by:

$$f_b = \frac{K_{ab}10^{pH}}{(1 + K_{ab}10^{pH})} \quad (2)$$

Here, $K_{ab} = [L_b]/[L_a]$, which is a constant related to the reversible interconversion between L_a^{3-} and L_b^{3-}. When this equilibrium is included into the intensity change with pH, Eq. (1) is rewritten as:

$$I = \frac{(I_{0b} \cdot K_{ab} \cdot 10^{pH} + I_{0a} + \sum I_n \cdot \beta_n \cdot 10^{-n\,pH})}{(K_{ab} \cdot 10^{pH} + 1 + \sum \beta_n \cdot 10^{-n\,pH})} \quad (3)$$

Here, I_{0b} and I_{0a} are emission intensities inherent in L_b^{3-} and L_a^{3-}, respectively. Least-squares curve fitting reproduces well the observed intensity vs. pH curve including the sharp change above pH 10.5 as shown in Fig. 3, in which the mol fractions of L_b^{3-} and L_a^{3-} are also plotted against pH. The logarithmic protonation constants determined by fluorometry (Table 2) are reasonable compared with the corresponding potentiometric data; log K_{p3} was not determinable by the spectroscopy because I_E was almost constant in the corresponding pH range. The inherent intensities presented in Table 2 show that the quite distinct I_E–pH profiles of the two DTPA derivatives are associated with the relative intensities of LH^{2-} and LH_2^- species. Another notable difference is that the conversion of L_a^{3-} to L_b^{3-} occurs in $(dtpa1py)H_3$, but does not in $(dtpa1mpy)H_3$.

The insertion of a CH_2 spacer between amide and pyrenyl groups causes differences in the acidity as well (Table 1). In the ^{1}H NMR spectra of $(dtpa1mpy)H_3$, protons *a*, *d* and *e* (labeled as shown in Scheme 1) exhibit downfield shifts with decreasing pD in the range of 8.3–12.9, and undergo line-broadening concurrently. A change in δ upon protonation, $\Delta\delta$, is 0.279 for *a*, 0.703 for *d*, and 0.537 for *e*; a figure of δ vs. pD plots is available as Supplementary Materials (Fig. S1). The curve fitting of the δ vs. pH plots has determined the logarithmic protonation constant in D_2O as log K_{D1} = 10.3, which is larger than the value 10.0 reported for $(dtpa1py)H_3$ [27], as predicted from their first protonation constants determined by potentiometry (Table 1). The ratio of chemical shift changes, $\Delta\delta(b)/\Delta\delta(d)$, is 0.04/0.70 for $(dtpa1mpy)H_3$ is very small compared to 0.11/0.70 of $(dtpa1py)H_3$. Since the $\Delta\delta(j)$ is proportional to proton population on nitrogen bonded to CH(*j*), the $\Delta\delta(b)/\Delta\delta(d)$ values show that the acidic protonation in the LH^{2-} species is concentrated on the central nitrogen to a larger extent in $(dtpa1mpy)H_3$ than in $(dtpa1py)H_3$. The insertion of a CH_2 spacer enhances the basicity of the central nitrogen, which may be one of the controlling factors on the conformation of the interlinking chain.

Geometry optimization was attempted to confirm the effect of the CH_2 spacer, but it was unsuccessful because the DTPA chain is so flexible to yield a number of local energy minima. For this reason, the corresponding EDTA derivatives have been studied as simpler model compounds as described in the following sections although characterizations by NMR and potentiometry are difficult because of the bare water solubility.

3.2. Luminescence of (edta1mpy)H_2

Fig. 4 shows the emission spectra of $(edta1mpy)H_2$ (**4**) at different pH values. A pyrene excimer band is observed at 475 nm with a shoulder at 490 nm, and a group of sharp monomer bands are between 370 and 420 nm. The excimer-to-monomer intensity

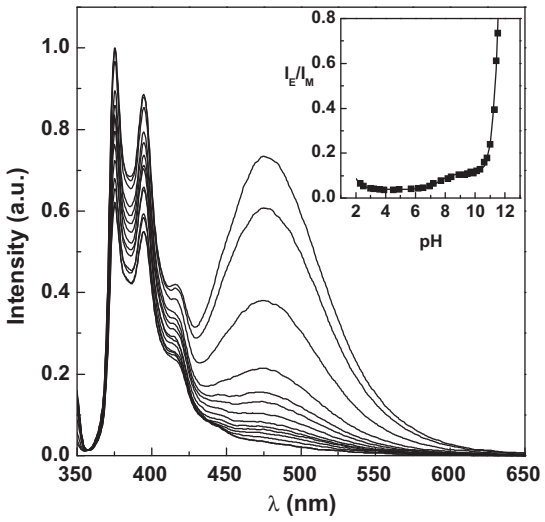

Fig. 4. Emission spectra of $(edta1mpy)H_2$ in aqueous solution at selected pH values. The spectral intensities are normalized to the peak maximum of the most intense spectrum. The excitation wavelength, λ_{exc} is 342 nm, and the concentration 1×10^{-6} M. Inset: excimer-to-monomer intensity ratio I_E/I_M as a function of pH. The solid line was obtained by curve fitting with Eq. (3).

ratio I_E/I_M was 0.45 at pH = 11.7, and decreased with decreasing pH in two steps. Protonation scheme in this compound was difficult to study, because the water solubility is too low for ^{1}H NMR and potentiometry. However, the first protonation on the L^{2-} species is supposed to occur at amino nitrogen of the EDTA units around pH 7, as reported for many EDTA bis(amide) derivatives [31–34]. The first protonation is, therefore, responsible for the spectral change around pH 7.5; the sharp spectral change above pH 11 is related to amide group as elucidated above for $(dtpa1py)H_3$. Least-square calculation based on Eq. (3) reproduces well the observed pH dependence of the emission intensity (inset in Fig. 4), giving $\log K_{ab}$ and $\log K_{p1}$ values shown in Table 2. The change in the intensity below pH 3 gives a logarithmic protonation constant ~0.1, which is extremely small compared with the values ~3 predicted for protonation at carboxylate oxygen. Probably, protonation at carboxylate oxygen does not influence the emission intensity so that the inherent intensities of the LH^- and LH_2 are identical to each other, and hence $\log K_{p2}$ is not determinable by fluorometry; the intensity change below pH 3 is caused by the third protonation that yields the LH_3^+ species.

The pH dependence of the emission intensity has a trend similar to that reported for $(edta1py)H_2$ (Fig. S2 in Supplementary Materials). However, the spectral change related to the first protonation in $(edta1mpy)^{2-}$ species occurs at pH lower than that in $(edta1py)^{2-}$ species: the I_E vs. pH plot gives $\log K_{p1} = 7.43$ for $(edta1mpy)H_2$ and 8.19 for $(edta1py)H_2$. The insertion of methylene group, therefore, lowers the basicity of amino nitrogen. Another effect of the CH_2 spacer is that the efficiency in excimer formation is reduced; while the excimer-to-monomer intensity ratio I_E/I_M amounts to ~5 for $(edta1py)H_2$ in basic media, the I_E/I_M value of $(edta1mpy)H_2$ is only 0.5 at largest.

The excitation spectra were monitored at 480 nm (corresponding to the excimer emission peak) and 375 nm (the monomer emission peak) at different pH values (Fig. S3). The set of bands related to the excimer emission exhibits a red shift (about 5 nm) and line broadening compared with that related to the monomer emission in the spectral region of 250–350 nm, suggesting that the emission at 480 nm may be due to a static excimer. However, the difference between monomer- and excimer-related spectra is less pronounced than that found for $(edta1py)H_2$ [27]. This fact shows that the conformation in the ground state of $(edta1mpy)H_2$ is less favorable for the formation of a static excimer than in $(edta1py)H_2$, in consistency with the lower I_E/I_M value of the former.

3.3. Optimized geometries of EDTA derivatives; possible conformations of DTPA derivatives

The geometry optimization has been carried out on the completely deprotonated species L^{2-} of $(edta1py)H_2$ and $(edta1mpy)H_2$, to explain the difference between their emission properties in relation to conformations in the ground state. The chain that links two pyrenyl groups is short enough for definitive optimization, but the inclusion of carboxymethyl group results in a number of local minima so that many conformations are obtained with small energy differences. Preliminary optimization was, therefore, carried out with the Hartree–Fock HF/3-21G(d) method, and some geometries having a low energy minimum and a C_2 symmetry were selected for further optimization on the basis of density functional theory with the B3LYP/6-31G(d) basis set implemented in Gaussian 03 [35]. Even after the refinement, energy differences among the geometries remained small. In any possible geometries obtained for both compounds, however, two pyrene rings basically face each other and orient toward the same direction with respect to the interlinking chain, as displayed in Fig. 5, which represents a geometry having the lowest energy minimum for each compound.

In the structure of the $(edta1py)^{2-}$ species, two pyrene rings are arranged almost parallel to each other with an angle of 5° between the ring planes and the closest C–C contact of 3.8 Å at C(9) and C(9′), and are slipped away with a distance of 8.3 Å between the ring centers; the same type of contact has been obtained by optimization without carboxylate groups [27]. This parallel ring orientation is responsible for the formation of a static excimer in the ground state, as suggested from the excitation spectrum [27]. In the structure obtained for the $(edta1mpy)^{2-}$ species, the pyrene–CH_2–amide linkage is kinked at the methylene carbon so that the relative orientation of the ethylenediamine chain axis and pyrene ring plane is altered from that in the $(edta1py)^{2-}$ species. Moreover, two pyrene rings are on a larger slant with an angle of 17.5° between the ring planes, and are more distant from each other with the distance 10.6 Å between the ring centers and the closest C–C contact 7.6 Å at C(2) and C(2′). Though the highly hydrophobic rings may move closer toward each other in aqueous media, the inter-pyrene distance is still longer than that in $(edta1py)H_2$. This looser contact of the pyrene rings in $(edta1mpy)H_2$ is unfavorable for the formation of a static excimer, and interprets the lower excimer-emission efficiency concluded from the emission and excitation spectra.

The structure of the DTPA derivative is difficult to optimize because the DTPA-based interlink is too long and flexible. Obviously, however, the pyrene–CH_2–amide linkage defines the orientation of pyrenyl rings in $(dtpa1mpy)H_3$ as well, to make the I_E–pH profile different from that of $(dtpa1py)H_3$. The order of the inherent intensities, $I_E(LH) > I_E(La) > I_E(LH_2)$, for $(dtpa1py)H_3$ has been interpreted in connection with the protonation scheme as illustrated schematically in Fig. 6: (1) protonation on the La^{3-} species leads to hydrogen bonding between amino nitrogen atoms in the LH^{2-} species so that the aliphatic chain is rigid and short to facilitate excimer formation in the protonated species; (2) the further protonation on amino nitrogen to form the LH_2^- species induces electrostatic repulsion so that the chain is stretched unfavorably for excimer formation [27]. The conformational change of the DTPA chain by protonation in $(dtpa1mpy)H_3$ is supposed to occur in the same manner as in $(dtpa1py)H_3$. However, the order of the inherent intensities of $(dtpa1mpy)H_3$ is $I_E(L) > I_E(LH_2) > I_E(LH)$, which is quite different from that of $(dtpa1py)H_3$. Probably, the pyrene–CH_2–amide linkage relocates two pyrene rings to the opposite directions unfavorably for excimer formation in the LH^{2-}

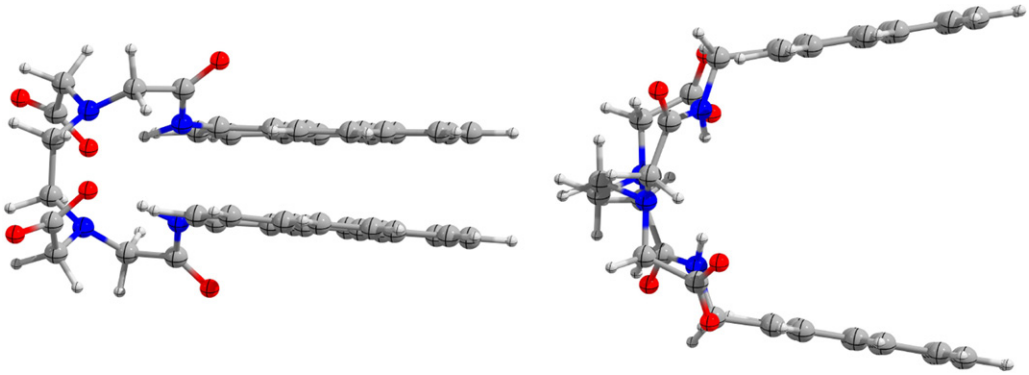

Fig. 5. Structures optimized for the L^{2-} species of $(edta1py)H_2$ (left) and $(edta1mpy)H_2$ (right) by B3LYP/6-31G(d) method. Both structures have a C_2 symmetry.

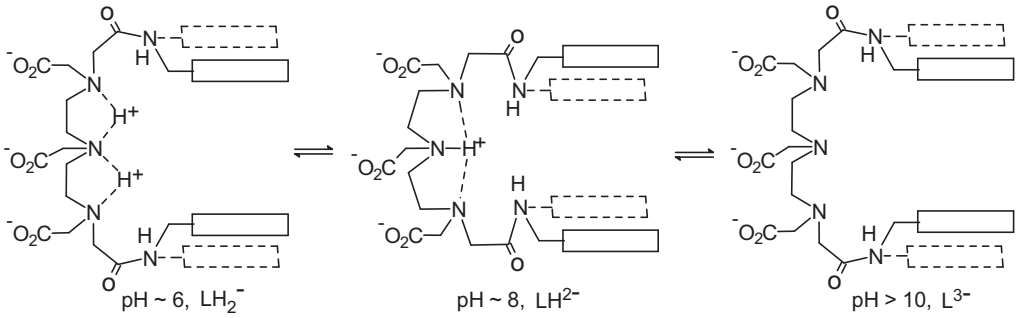

Fig. 6. Possible changes in the orientation of pyrene rings with pH in $(dtpa1py)H_3$ and $(dtpa1mpy)H_3$. The rectangles show pyrene disks, which are drawn by dotted line for $(dtpa1py)H_3$ and solid line for $(dtpa1mpy)H_3$.

species, as illustrated in Fig. 6; on the other hand, the CH_2 spacer has a reverse effect to make pyrene rings closer in the L^{3-} and LH_2^- species. Even in the L^{3-} and LH_2^- species of $(dtpa1mpy)H_3$, the pyrene–pyrene interaction is supposed to be weaker than in the LH^{2-} species of $(dtpa1py)H_3$. The efficiency in the excimer formation is, therefore, lower in the former, as observed in the emission spectra, although the overall fluorescence intensity is much higher. In both DTPA derivatives, the pyrene–pyrene contact is supposed to be looser than in $(edta1py)H_2$, because of the longer interlinking chain in the formers. In fact, the excitation spectra of $(dtpa1py)H_3$ has been reported to suggest that the excimer emission originates from a dynamic excimer formed in the excited state rather than a static excimer formed in the ground state [27]. Basically the same conclusion can be derived for $(dtpa1mpy)H_3$, from the excitation spectra, in which the relation between the excimer- and monomer-related spectra is similar to that observed for $(dtpa1py)H_3$ and $(edta1mpy)H_2$ (Fig. S4). The DTPA chain is too long to form a close face-to-face stack of pyrene in the ground state, but is flexible enough to form an excimer in the excited state.

3.4. Luminescence of $(ttha1py)H_4$

The emission spectra of $(ttha1py)H_4$ (**3**) exhibits an intense excimer band at 487 nm and vibronically structured monomer bands between 393 and 414 nm in basic solutions (Fig. 7). The excimer-to-monomer intensity ratio I_E/I_M is about 5 at pH = 11.4, and decreases with decreasing pH down to about 1 at pH = 10. Fig. 8 shows a plot of the excimer emission intensity I_E against pH, together with the species distribution obtained from potentiometric data (Table 1). The pH dependence of the emission intensity is well correlated with the species distribution except for the pH range above 10.5. A sharp change in I_E takes place at pH much higher than that corresponding to the log K_{p1} values. This discrepancy is ascribable to the response of amide group to a change in environment, as proposed for $(dtpa1py)H_3$. The I_E vs. pH plot can be well interpreted by Eq. (3) with the equilibrium constants

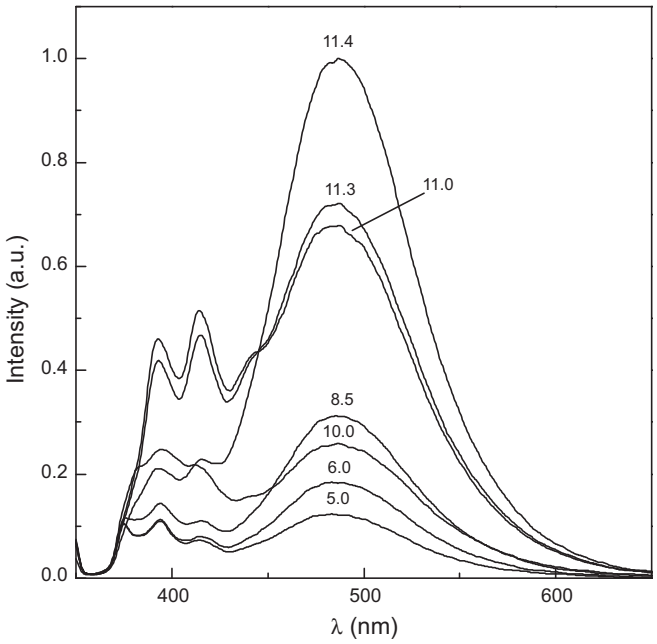

Fig. 7. Emission spectra of $(ttha1py)H_4$ in aqueous solution at selected pH values. The spectral intensities are normalized to the peak maximum of the most intense spectrum. The excitation wavelength, λ_{exc} is 342 nm, and the concentration 1×10^{-6} M.

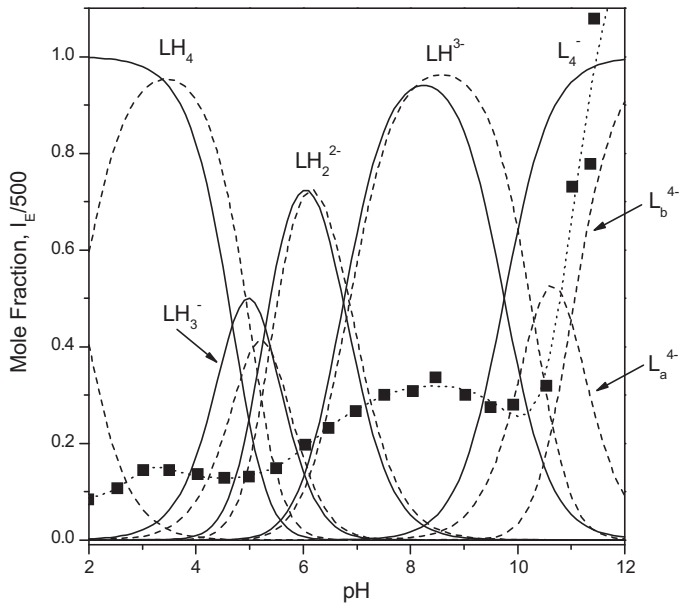

Fig. 8. Excimer emission intensity I_E (squares) of (ttha1py)H_4 as a function of pH, and mole fractions of the species determined by potentiometry (solid lines) and fluorometry (dashed lines). The dotted line is the best fit obtained by Eq. (3) with log K_p values in Table 2.

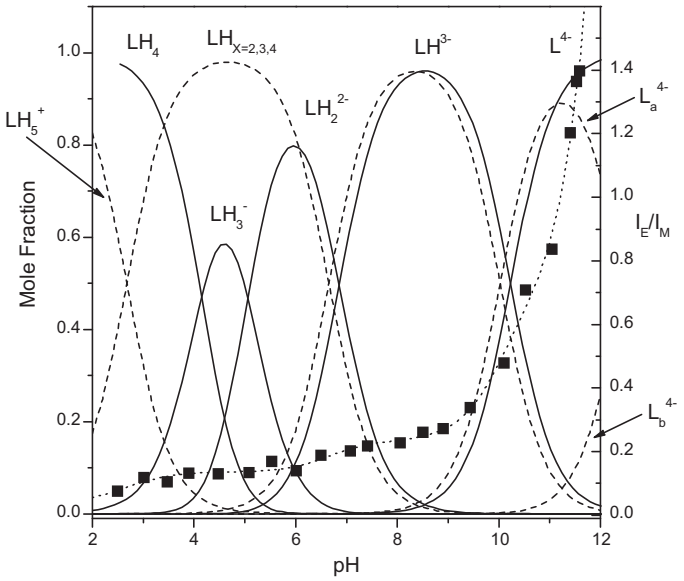

Fig. 9. Mole fraction distribution of the different species of (ttha1mpy)H_4 obtained by potentiometry (solid lines) and fluorescence (dashed lines) and excimer-to-monomer intensity ratio I_E/I_M (squares) as a function of pH. The dotted line is the fitting curve in accordance with Eq. (3). For log K_p values see Tables 1 and 2. The dashed line centered at pH ~ 5 shows the sum of the mole fractions of the LH_2^{2-}, LH_3^- and LH_4 species, because log K_{p3} and log K_{p4} are unable to be determined due to the insensitiveness of the fluorescence to the protonation processes in the pH range 4–6.

shown in Table 2; the obtained values are reasonable compared with the corresponding potentiometric data. The relative intensities of the species indicate that the trend of the intensity toward pH resembles that of (dtpa1py)H_3 (Table 2): (1) the mono-protonated species LH has a higher efficiency for excimer formation than the poly-protonated species LH_n; (2) deprotonation from LH weakens excimer emission at the initial stage of the formation of the L^{4-} species; (3) with the further increase of pH, the totally deprotonated species L^{4-} undergoes a conformational change due to the sensitiveness of amide group to the pH change; (4) the resulting species L_b exhibits an extremely high efficiency for excimer formation.

Excitation spectra monitored at the wavelengths of the excimer emission (480 nm) and the monomer emission (375 nm) show a striking difference in the high-energy region of 200–250 nm; an excimer-related band is centered at about 241 nm whereas the corresponding monomer-related band is at 217 nm (Fig. S5). This large red shift of the excimer-related band is evidence that the 480 nm emission band is due to a static excimer formed in the ground state. This conclusion is supported by the UV–Vis absorption bands that are broadened in the whole pH window (Fig. S6). The molecule is flexible enough to form a well-defined pyrene–pyrene contact due to the hydrophobic effect in aqueous media.

The effects of protonation on the excimer emission can be explained by a scheme similar to that schematically shown for (dtpa1py)H_3 in Fig. 6, as follows. Acidic hydrogen in the fluorescent species LH^{3-} is located at the central amino nitrogen because the ^{1}H NMR signals of protons *d*, *e* and *f* undergo downfield shifts simultaneously with decreasing pH (Fig. S7); the curve fitting of the δ vs. pD plot gives log K_{D1} = 10.70. The added acidic hydrogen is shared by two central nitrogen atoms, which are chemically equivalent. A consequent hydrogen bond makes rigid the central region of the aliphatic chain; this rigidity may be related to the intensity change of the excimer emission in the pH range of 8–10. The next protonation occurs on the terminal amino nitrogen atoms, and the resulting electrostatic repulsion between the protons stretches the interlinking chain so that the conformation in the LH_2^{2-} species is less favorable for excimer formation.

3.5. Luminescence of (ttha1mpy)H_4

The emission spectrum of (ttha1mpy)H_4 (**6**) exhibits excimer and monomer bands at the same wavelengths as observed for other pyrenyl derivatives (Fig. S8). However, the intensity profile is distinct from that of (ttha1py)H_4. The intensity of the excimer emission is almost identical with that of the monomer intensity around pH 12. As pH decreases, the excimer band is weakened sharply, whereas the monomer band is strengthened slightly: I_E/I_M is only 0.2 at pH = 8 in contrast to I_E/I_M = 1.4 at pH = 11.6 (Fig. 9). The change in I_E is monotonous, and a plateau corresponding to a possible protonation is not found in the I_E vs. pH plot (Fig. S8). On the other hand, the I_E/I_M vs. pH plot shows two well-defined plateaus to make it possible to determine at least three protonation constants, although a clear change is still undetectable in the pH range 4–6 where the formation of LH_3^- and LH_4 is expected from the potentiometric data (Fig. 9). The sharp change above pH 11 does not correspond to any protonation process predicted by potentiometry, and is attributable to the effect of amide group as proposed for (ttha1py)H_4. Least-squares calculations based on Eq. (3) gave three protonation constants and K_{ab} shown in Table 2.

The I_E/I_M ratios are smaller in (ttha1mpy)H_4 than in (ttha1py)H_4. The weaker excimer emission is ascribable to a weaker intramolecular interaction between the pyrene units. In fact, the excimer-related excitation spectra are not significantly different from the monomer-related excitation spectra (Fig. S9), in contrast to the excitation spectra of (ttha1py)H_4. This spectral difference is obviously caused by the insertion of the methylene spacer, as explained for the EDTA and DTPA derivatives.

The effect of the CH_2 spacer is clearly observed by ^{1}H NMR; the spectra at selected pH values are represented in Fig. 10. The most notable feature of the ^{1}H NMR spectra is that a methylene proton signal located at $\delta \sim 1.8$ at pD ~ 12 shifts upfield with decreasing pD and reaches δ as small as 0.6 at pD ~ 9; the δ vs. pD plot of the signal shows a clear minimum at pD ~ 9 (Fig. 11). A similar but smaller

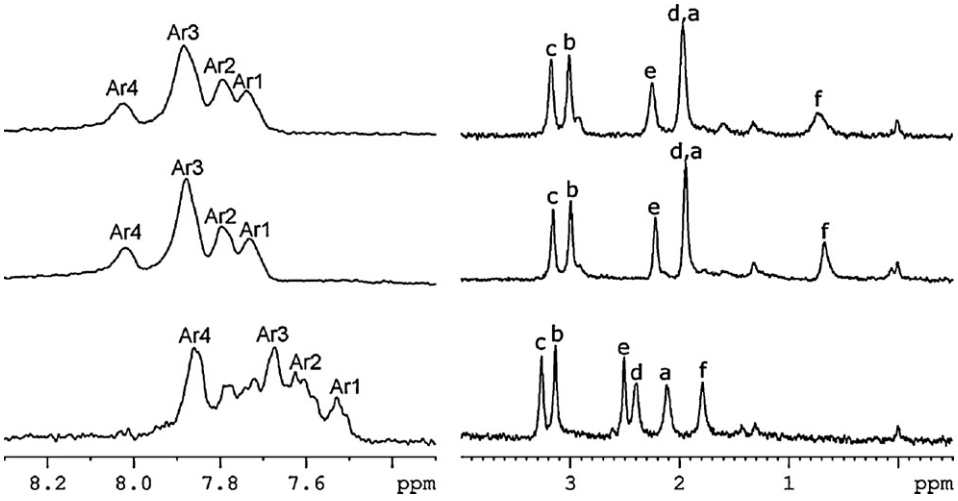

Fig. 10. ^{1}H NMR spectra of CH_2 and aromatic protons of (ttha1mpy)H_3 at different pD values. From top to bottom: 8.8, 9.46 and 12.37. For the labels of CH_2 protons see Scheme 1. Aromatic proton signals are labeled as an aid for tracing the shifts, which are plotted in Fig. 11.

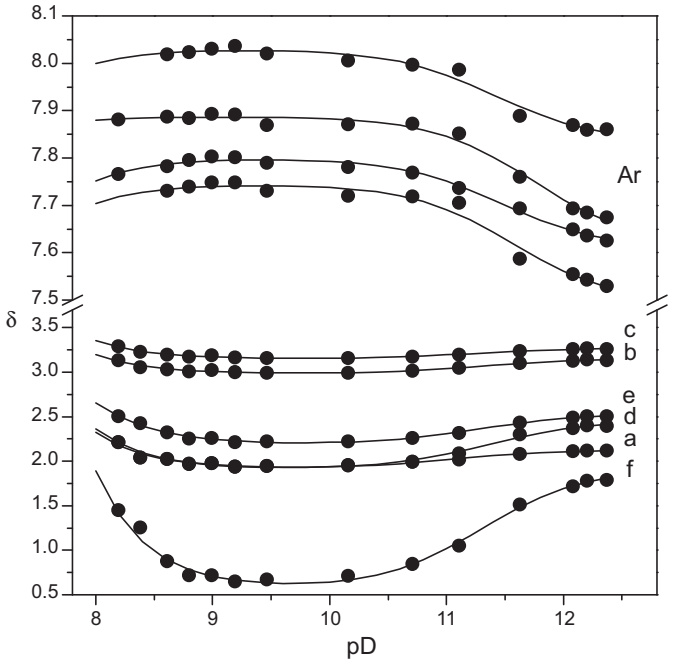

Fig. 11. pD dependence of ^{1}H NMR chemical shifts (referenced to DSS) of (ttha1mpy)H_4. For the labels of CH_2 protons see Scheme 1. The solid lines are the best fit based on equation $\delta_j(\mathrm{pD}) = \{\delta_{j0} + \sum_n \delta_{jn} \cdot \beta_{\mathrm{D}n} \cdot 10^{-n \cdot \mathrm{pD}}\} / \{1 + \sum_n \beta_{\mathrm{D}n} \cdot 10^{-n \cdot \mathrm{pD}}\}$ where $\beta_{\mathrm{D}n}$ is the nth overall protonation constant in D_2O, and δ_{j0} and δ_{jn} are the δ_j values of (ttha1mpy)$^{4-}$ and (ttha1mpy)$H_n^{(4-n)-}$, respectively: $\log K_{\mathrm{D1}} = 11.4$ and $\log K_{\mathrm{D2}} \sim 7$; $\delta_{f0} = 1.9$ and $\delta_{f1} = 0.57$.

change is observed for other signals. In the pD range of 9–12, the first protonation is supposed to occur on amino nitrogen on the basis of the $\log K_{\mathrm{p1}}$ value. However, the direction of the shift with pD is opposite to that caused by a simple protonation process, in which protonation on nitrogen in NCH_2 causes a downfield shift (or an increase in δ) of the adjacent proton as observed for (ttha1py)H_4 and other derivatives. Furthermore, the δ value of 0.6 is extremely small compared with the value ~3 of common NCH_2 proton signals, and the difference ~2.4 between the δ values is much larger than that predicted for protonation at the adjacent nitrogen atom [36]. This unusual δ value and novel pH dependence can be interpreted by the ring-current effect of pyrene. A chemical shift due to a ring current, δ_{rc}, of a pyrene ring can be calculated as the sum of dipole fields induced by component hexagons [37]:

$$\delta_{\mathrm{rc}} = -27.6 \sum_j (1 - 3\cos^2\theta_j) R_j^{-3} \quad (4)$$

Here, R_j is distance (in Å) between the resonant proton and the center of hexagon j, and θ_j is the angle between the vector $\boldsymbol{R}_j$ and the normal to the hexagon center. The value of δ_{rc} is given in Table 3 for a proton located above a selected position of a pyrene ring at a given distance from the ring plane. The effect of ring current is large enough to result in the observed δ as small as 0.6; the proton showing this signal is located above the pyrene ring plane. At least two other CH_2 groups of the TTHA chain are under influence of the ring current field of pyrene at pD where LH^{3-} species is formed. The acidic proton in LH^{3-} is expected to be distributed on two chemically equivalent nitrogen atoms in $NCH_2(f)CH_2(f)N$, as found for (ttha1py)H_4. Probably, the resulting hydrogen bonding folds the aliphatic chain in between two pyrene disks, as illustrated for LH^{3-} in Fig. 12. In such a structure, the central ethylene group $NCH_2(f)CH_2(f)N$ is located closest to the center of the pyrene ring among the CH_2 protons. The change in δ caused by each pyrene ring is approximately −2.4/2 ppm. Comparison of this value with Table 3 suggests that $NCH_2(f)$ proton is located in the range of 4.5–5 Å from the ring plane above either of the centers of the pyrene ring and hexagons. On the other hand, the $CH_2(c)$ attached to amide group is supposed to reside outside of the pyrene disk so that the ring current effect is negligible on the proton; the aliphatic proton signal of the largest δ is assignable to $CH_2(c)$. Other proton signals are assigned tentatively as shown in Fig. 10 on the basis of the possible locations of the protons. As the second protonation occurs below pD 9, the δ value of every proton increases. In the LH_2^{2-} species, therefore, the CH_2 protons are less influenced by the ring current field. Two acidic hydrogen atoms are distributed over four nitrogen atoms, and the resulting hydrogen bonding stretches the aliphatic chain because of electrostatic repulsion between the acidic protons, so that the CH_2 protons reside distant from the ring center. Thus, the equilibrium between the LH^{3-} and LH_2^{2-} species is accompanied by an accordion-like conformational change, as illustrated in Fig. 12. As a result, the proton signals show downfield shifts with decreasing pD below 9. Both structures of the LH^{3-} and LH_2^{2-} species are unfavorable for excimer formation to quench the excimer emission in the low pH range. The δ values observed for the L^{4-} species show that the aliphatic chain is located outside the ring current field. The aromatic protons show decreases in δ with increasing

Table 3
Ring current shift, δ_{rc} (ppm), calculated for a proton that resides above a selected position of a pyrene ring at a given height Z (Å) from the ring face.

Z	M	A	B	Cα	Cβ	Cγ	Hα	Hβ	Hγ
3.0	−3.72	−2.84	−3.23	−1.37	−1.17	−1.45	−0.38	−0.28	−0.38
3.5	−2.80	−2.06	−2.39	−1.16	−0.98	−1.25	−0.45	−0.33	−0.47
4.0	−2.13	−1.57	−1.83	−0.97	−0.82	−1.06	−0.46	−0.35	−0.49
4.5	−1.64	−1.23	−1.43	−0.81	−0.69	−0.89	−0.44	−0.34	−0.47
5.0	−1.28	−0.98	−1.13	−0.68	−0.59	−0.75	−0.41	−0.32	−0.44

M, center of pyrene ring; A, center of hexagon A involving Cα; B, center of hexagon B involving Cγ; Cα = C1, C3, C6, C8; Cβ = C2, C7; Cγ = C4, C5, C9, C10.

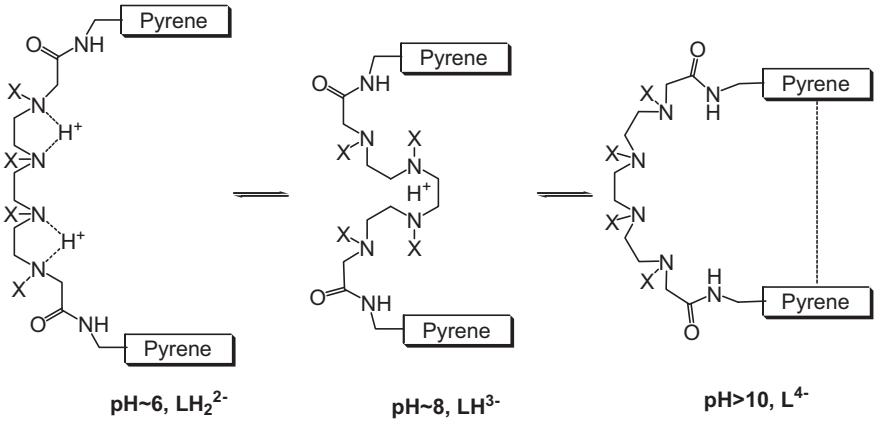

Fig. 12. A possible conformational change of the aliphatic interlink upon protonation in (ttha1mpy)H_4. The rectangles show pyrene rings, and X = $CH_2CO_2^-$.

pD in the region where equilibrium occurs between LH^{3-} and L^{4-} species (Figs. 10 and 11). This change in δ indicates that the pyrene rings are mutually influenced through the ring-current field in the L^{4-} species, suggesting the close contact of the pyrene rings. The totally deprotonated aliphatic chain is so flexible that the face-to-face contact of the pyrene rings is possible in aqueous media, giving rise to a weak but well-defined excimer band of the L^{4-} species at pH ∼10. As pH increases further, the pyrene rings become closer to each other, as suggested by the chemical shifts of pyrene protons, to exhibit even stronger excimer emission.

The novel conformation in the LH^{3-} species of the methylpyrenyl derivative is due to the amide–CH_2–pyrenyl linkage, which is bent at the methylene carbon to make the aliphatic chain oriented toward the face of the pyrene ring. In contrast, the amide–pyrenyl linkage in (ttha1py)H_3 is stretched on the pyrene ring plane because of the conjugation of the two groups, and hence the effective length is too short to make the folded structure.

4. Conclusions

The interlinking chain between the chromophores alters its conformation upon protonation on the amino nitrogen in the polyaminopolycarboxylic acid derivatives. This effect combined with that of amide group results in the repeated "on–off" profiles of excimer emission against pH. The number of the on–off cycle respondent to protonation increases with increasing the number of amino nitrogen atoms involved in the polyamino chain, although the effect is attenuated with the protonation step. Another effect on emission is caused by the CH_2 spacer between the amide and pyrenyl groups in the methylpyrenyl derivatives. The stacking of pyrene rings in a molecule is defined in part by the planarity of the pyrene and amide groups. The relative orientation of these groups is controlled by the CH_2 spacer so that the on–off cycles in the DTPA- and TTHA-based methylpyrenyl derivatives are reversed to those of the corresponding pyrenyl derivatives. These novel properties are a result of combined effects of the chain length, the number of protonation sites, the acidity of amide group and its orientation.

Acknowledgments

This work was supported in part by the Consejo Nacional de Ciencia y Tecnología de México (CONACYT, Project No. 79272). The NMR spectrometer is operated under the support of the Secretaría de Educación Publica, México (SES-SEP, programs No. P/PIFI 2008-26 and No. P/FPCU2008-07). The authors thank Jesús Eduardo Ávila Manzanares, Edel Carrillo Moreno and Moisés Vera Pacheco for technical assistance. R.P.-G. is indebted to CONACYT for graduate scholarship.

Appendix A. Supplementary data

Supplementary data associated with this article can be found, in the online version, at 10.1016/j.jphotochem.2011.01.022.

References

[1] F.M. Winnik, Photophysics of preassociated pyrenes in aqueous polymer solutions and in other organized media, Chemical Reviews 93 (1993) 587–614.
[2] S.K. Kim, J.H. Bok, R.A. Bartsch, J.Y. Lee, J.S. Kim, A fluoride-selective PCT chemosensor based on formation of a static pyrene excimer, Organic Letters 7 (2005) 4839–4842.
[3] I. Aoki, H. Kawabata, K. Nakashima, S. Shinkai, Fluorescent calix[4]arene which responds to solvent polarity and metal ions, Journal of the Chemical Society, Chemical Communications (1991) 1771–1773.
[4] T. Jin, K. Ichikawa, T. Koyama, A fluorescent calix[4]arene as an intramolecular excimer-forming Na^+ sensor in nonaqueous solution, Journal of the Chemical Society, Chemical Communications (1992) 499–501.
[5] S.K. Kim, S.H. Lee, J.Y. Lee, J.Y. Lee, R.A. Bartsch, J.S. Kim, An excimer-based, binuclear, on–off switchable calix[4]crown chemosensor, Journal of the American Chemical Society 126 (2004) 16499–16506.
[6] K. Kubo, N. Kato, T. Sakurai, Synthesis and complexation behavior of diaza-18-crown-6 carrying two pyrenylmethyl groups, Bulletin of the Chemical Society of Japan 70 (1997) 3041–3046.
[7] H.J. Kim, D.T. Quang, J. Hong, G. Kang, S. Ham, J.S. Kim, Ratiometry of monomer/excimer emissions of dipyrenyl calix[4]arene in aqueous media, Tetrahedron 63 (2007) 10788–10792.

[8] Y. Nakahara, Y. Matsumi, W. Zhang, T. Kida, Y. Nakatsuji, I. Ikeda, Fluorometric sensing of alkaline earth metal cations by new lariat ethers having plural pyrenylmethyl groups on the electron-donating sidearms, Organic Letters 4 (2002) 2641–2644.
[9] J. Xie, M. Ménand, Stephane, R. Métivier, Synthesis of bispyrenyl sugar-aza-crown ethers as new fluorescent molecular sensors for Cu(II), The Journal of Organic Chemistry 72 (2007) 5980–5985.
[10] L. Prodi, R. Ballardini, M.T. Gandolfi, R. Roversi, A simple fluorescent chemosensor for alkaline-earth metal ions, Journal of Photochemistry and Photobiology A: Chemistry 136 (2000) 49–52.
[11] Y. Suzuki, T. Morozumi, H. Nakamura, M. Shimomura, T. Hayashita, R.A. Bartsh, New fluorimetric alkali and alkaline earth metal cation sensors based on non-cyclic crown ethers by means of intramolecular excimer formation of pyrene, The Journal of Physical Chemistry B 102 (1998) 7910–7917.
[12] J.-S. Yang, C.-S. Lin, C.-Y. Hwang, Cu^{2+}-induced blue shift of the pyrene excimer emission: a new signal transduction mode of pyrene probes, Organic Letters 3 (2001) 889–892.
[13] Y. Kakizawa, T. Akita, H. Nakamura, Syntheses and complexing behavior of new fluorescent reagents for alkaline earth metal ions, Chemistry Letters 22 (1993) 1671–1674.
[14] J. Kollár, P. Hrdlovic, S. Chmela, Spectral properties of bichromophoric pyrene derivatives; monomer vs. excimer fluorescence, Journal of Photochemistry and Photobiology A: Chemistry 214 (2010) 33–39.
[15] J.S. Kim, M.G. Choi, K.C. Song, K.T. No, S. Ahn, S.-K. Chang, Ratiometric determination of Hg^{2+} ions based on simple molecular motifs of pyrene and dioxaoctanediamide, Organic Letters 9 (2007) 1129–1132.
[16] H.-C. Hung, C.-W. Cheng, I.T. Ho, W.-S. Chung, Dual-mode recognition of transition metal ions by bis-triazoles chained pyrenes, Tetrahedron Letters 50 (2009) 302–305.
[17] Y. Zhou, C.-Y. Zhu, X.-S. Gao, X.-Y. You, C. Yao, Hg^{2+}-selective ratiometric and "off–on" chemosensor based on the azadiene–pyrene derivative, Organic Letters 12 (2010) 2566–2569.
[18] R. Martínez, A. Espinosa, A. Tárraga, P. Molina, A new bis(pyrenyl)azadiene-based probe for the colorimetric and fluorescent sensing of Cu(II) and Hg(II), Tetrahedron 66 (2010) 3662–3667.
[19] R. Martínez, A. Espinosa, A. Tárraga, P. Molina, New Hg^{2+} and Cu^{2+} selective chromo- and fluoroionophore based on a bichromophoric azine, Organic Letters 7 (2005) 5869–5872.
[20] I. Aoki, T. Harada, T. Sakaki, Y. Kawahara, S. Shinkai, Fluorescence 'reading-out' of the molecular-recognition process, Journal of the Chemical Society, Chemical Communications (1992) 1341–1345.
[21] B. Pedras, H.M. Santos, L. Fernandes, B. Covelo, A. Tamayo, E. Bértolo, J.L. Capelo, T. Avilés, C. Lodeiro, Sensing metal ions with two new azomethine-thiophene pincer ligands (NSN): fluorescence and MALDI-TOF-MS applications, Inorganic Chemistry Communications 10 (2007) 925–929.
[22] H.N. Lee, N.J. Singh, S.K. Kim, J.Y. Kwon, Y.Y. Kim, K.S. Kim, J. Yoon, New imidazolium systems bearing two pyrene groups as fluorescent chemosensors for anions and anion induced logic gates, Tetrahedron Letters 48 (2007) 169–172.
[23] F. Sancenón, A.B. Descalzo, J.M. Lloris, R. Martínez-Máñez, T. Pardo, M.J. Seguí, J. Soto, Open-chain polyazaalkanes functionalised with pyrene groups as sensing fluorogenic receptors for metal ions, Polyhedron 21 (2002) 1397–1404.
[24] C. Lodeiro, J.C. Lima, A.J. Parola, J.S. Seixas de Melo, J.L. Capelo, B. Covelo, A. Tamayo, B. Pedras, Intramolecular excimer formation and sensing behavior of new fluorimetric probes and their interactions with metal cations and barbituric acids, Sensors and Actuators B: Chemical 115 (2006) 276–286.
[25] Y. Shiraishi, Y. Tokitoh, T. Hirai, pH- and H_2O-driven triple-mode pyrene fluorescence, Organic Letters 8 (2006) 3841–3844.
[26] Y. Shiraishi, K. Ishizumi, G. Nishimura, T. Hirai, Effects of metal cation coordination on fluorescence properties of a diethylenetriamine bearing two end pyrene fragments, The Journal of Physical Chemistry B 111 (2007) 8812–8822.
[27] L. Machi, I.C. Muñoz, R. Pérez-González, M. Sánchez, M. Inoue, Pyrene bichromophores composed of polyaminopolycarboxylate interlink: pH response of excimer emission, Supramolecular Chemistry 21 (2009) 665–673.
[28] B. Achour, J. Costa, R. Delgado, E. Garrigues, C.F.G.C. Geraldes, N. Korber, F. Nepveu, M.I. Prata, Triethylenetetramine-*N*,*N*,*N*′,*N*″,*N*‴,*N*‴′-hexaacetic acid (TTHA) and TTHA-bis(butanamide) as chelating agents relevant to radiopharmaceutical applications, Inorganic Chemistry 37 (1998) 2729–2740.
[29] A.K. Covington, M. Paabo, R.A. Robinson, R.G. Bates, Use of the glass electrode in deuterium oxide and the relation between the standardized pD (paD) scale and the operational pH in heavy water, Analytical Chemistry 40 (1968) 700–706.
[30] M. Inoue, Excel® Worksheets for Spectrometry, Universidad de Sonora, 2009.
[31] L. Machi, H. Santacruz, M. Sánchez, M. Inoue, Bichromophoric naphthalene derivatives of ethylenediaminetetraacetate: fluorescence from intramolecular excimer, protonation and complexation with Zn^{2+} and Cd^{2+}, Supramolecular Chemistry 18 (2006) 561–569.
[32] L. Machi, H. Santacruz, M. Sánchez, M. Inoue, Cd^{2+}-sensiting bichromophore: excimer emission from an EDTA–methylnaphthalene derivative, Inorganic Chemistry Communications 10 (2007) 547–550.
[33] M.B. Inoue, L. Machi, I.C. Muñoz, S. Rojas-Rivas, M. Inoue, Q. Fernando, Metal–ligand interactions in benzodioxotetraaza-macrocyclic metal chelates, Inorganica Chimica Acta 324 (2001) 73–80.
[34] M.B. Inoue, I.C. Muñoz, M. Inoue, Q. Fernando, X-ray structures and fluorescence spectra of binuclear Zn^{2+} and Cd^{2+} complexes of an amide-based naphthalenophane, Inorganica Chimica Acta 300–302 (2000) 206–211.
[35] M. Frisch, G. Trucks, H. Schlegel, G. Scuseria, M. Robb, J. Cheeseman, J. Montgomery Jr., T. Vreven, K. Kudin, J. Burant, Gaussian 03, Revision B.05, Gaussian, Inc., Pittsburgh, PA, 2003.
[36] J.L. Sudmeier, C.N. Reilley, Nuclear magnetic resonance studies of protonation of polyamine and aminocarboxylate compounds in aqueous solution, Analytical Chemistry 36 (1964) 1698–1706.
[37] J.A. Pople, W.G. Schneider, H.J. Bernstein, High-resolution Nuclear Magnetic Resonance, McGraw-Hill, New York, 1959.